

This is the accepted manuscript made available via CHORUS. The article has been published as:

## Effects of Free Carriers on the Optical Properties of Doped CdO for Full-Spectrum Photovoltaics

Chao Ping Liu, Yishu Foo, M. Kamruzzaman, Chun Yuen Ho, J. A. Zapien, Wei Zhu, Y.J. Li, Wladek Walukiewicz, and Kin Man Yu

Phys. Rev. Applied **6**, 064018 — Published 28 December 2016

DOI: [10.1103/PhysRevApplied.6.064018](https://doi.org/10.1103/PhysRevApplied.6.064018)

# Free carrier effects on optical properties of doped CdO for full spectrum photovoltaics

Chao Ping Liu<sup>1</sup>, Yishu Foo<sup>1</sup>, M. Kamruzzaman<sup>1</sup>, Chun Yuen Ho<sup>1</sup>, J. A. Zapien<sup>1</sup>, Wei Zhu<sup>2,3</sup>, Y. J. Li<sup>2,4</sup>, Wlodek Walukiewicz<sup>2</sup>, and Kin Man Yu<sup>1\*</sup>

<sup>1</sup>Department of Physics and Materials Science, City University of Hong Kong, 83 Tat Chee Ave., Kowloon, Hong Kong

<sup>2</sup>Materials Sciences Division, Lawrence Berkeley National Laboratory, 1 Cyclotron Rd., Berkeley, CA 94720

<sup>3</sup>Department of Physics and Center for Physical Experiments, University of Science and Technology of China, Hefei, Anhui 230026 P. R. China.

<sup>4</sup>State Key Laboratory of Luminescent Materials and Devices, and Institute of Optical Communication Materials, South China University of Technology, Guangzhou 510641, China

\* corresponding: kinmanyu@cityu.edu.hk

## ABSTRACT

CdO based transparent conducting oxide thin films have great potential applications in optoelectronic devices due its high mobility, low resistivity and high transparency over a wide spectral range. In this work, we report results of a comprehensive study of optical properties of CdO thin films doped with different donors (In, Ga, V, Ti) with carrier concentration in the range of  $10^{20}$  to  $>10^{21}/\text{cm}^3$ . Variable angle spectroscopic ellipsometry (SE) studies revealed that the complex dielectric function of CdO thin films drastically depends on the carrier concentration. Specifically, with increasing carrier concentration, (1) the net effect of Burstein-Moss shift and band gap renormalization gives rise to an increase in the optical band gap from 2.6 to 3.2 eV; (2) the free carrier absorption coefficient at wavelength of 1200 nm increases from  $10^2$  to  $1 \times 10^4 \text{ cm}^{-1}$ ; (3) the refractive index decreases from 2.4 to 2.05 at 600 nm; (4) the high frequency dielectric constant reduces from 5.5 to 4.8. The SE results were analyzed with results from Hall measurements to obtain information on the electron effective mass and optical mobility of CdO thin films. The significantly higher effective mass of V and Ti doped CdO thin film is attributed to the modification of the conduction band due to anticrossing interaction between the localized d-levels of V and Ti atoms and the CdO conduction band extended states. The effective mass of In and Ga doped CdO increases with the electron concentration, consistent with the prediction from the nonparabolic conduction band model. We also found that the optical mobility  $\mu_{opt}$  is close to the Hall mobility  $\mu_{Hall}$  when the  $\mu_{Hall} < 60 \text{ cm}^2/\text{Vs}$ , while  $\mu_{opt} < \mu_{Hall}$  for materials with higher  $\mu_{Hall}$ .

## 1. INTRODUCTION

Transparent conductors are an essential component in many electronic devices including portable electronics, flat-panel displays, low-e windows and solar cells [1]. The most commonly used transparent conductors are wide gap metal oxides (transparent conducting oxides or TCOs) such as doped indium oxide, zinc oxide or tin oxide. Transparent conductors need to have low resistivity ( $\sim 10^{-4} \Omega\text{-cm}$ ) and high transparency ( $>85\%$ ) in the visible and near ultraviolet spectral range [1-2]. The current TCO market is dominated by indium oxides such as  $\text{In}_2\text{O}_3\text{:Sn}$  (ITO) due to their excellent electrical and optical performance [3,4]. Since indium is a rare element in the earth's crust, the high demand of ITO in various industries has driven up the price of Indium considerably. Hence there is a great incentive to find replacements for the expensive ITO [3-4]. One of these low cost alternatives is Aluminum doped Zinc oxide (AZO) [5] with electrical and optical properties approaching those of ITO.

Cadmium oxide (CdO) with rocksalt crystal structure (space group= $\text{Fm-3m}$ ) was one of the oldest TCO studied and has received a growing attention recently due to its high propensity for n-type doping and high electron mobility [6-13]. Previous studies have shown that native defects play a dominant role in electrical and optical properties of CdO. Based on hybrid density functional theory, Burbano et al. found that oxygen vacancy constitutes the dominate intrinsic donor defect, while the compensation by acceptor defects would not occur until its fermi level reaching 1.2 eV above the conduction band minimum [14]. Yu et al. performed thermal annealing studies of sputtered deposited CdO in  $\text{O}_2$  and  $\text{N}_2$  ambient and showed that the high electron concentration in sputter deposited films can be attributed to O related native defects [15].

High quality of CdO thin films can be grown by a variety of deposition methods. For instance, Yan *et al.* reported the epitaxial growth of CdO:Sn film on MgO (111) substrate by pulsed laser deposition, achieving a conductivity of  $4.2 \times 10^4 \text{ S/cm}$  and a mobility of  $609 \text{ cm}^2/\text{Vs}$  at a carrier concentration of  $4.74 \times 10^{20} \text{ cm}^{-3}$  [6]. Yu *et al.* demonstrated that doped CdO thin film deposited on glass substrates can exhibit high conductivity as well as high transparency in the visible to IR spectral range, making it an ideal transparent electrode for high efficiency multijunction photovoltaic devices [7]. Due to its large static dielectric constant ( $\epsilon_0=21.9$ ) [16], CdO has very high electron mobility because of reduced electron scattering through efficient screening of coulomb potentials of ionized donors. The high electron mobility allows for highly conductive CdO with relatively low electron concentration of mid  $10^{20}/\text{cm}^3$ , and therefore low free carrier absorption that enables high transparency up to  $>1200 \text{ nm}$  range [7,9,17].

For transparent conductor applications, CdO thin films with carrier concentration  $>\text{mid } 10^{20}/\text{cm}^3$  is needed to achieve a resistivity  $<\sim 10^{-4} \Omega\text{-cm}$ . Such high concentration of free carriers significantly alters optical properties of a semiconductor. For instance, the onset of band-edge absorption in degenerate semiconductor blueshifts due to the large amount of free carriers filling in the

conduction band. This effect is known as Burstein-Moss effect. At the same time, strong free carrier absorption would be present in the NIR spectral range, [18] and this will narrow the transmission window in the long wavelength regime.

For TCO materials, it is of great importance to understand the effect of free carriers on their opto-electronic properties [19-22]. Optical studies of TCOs were typically carried out using conventional transmittance/reflectance (T/R) [7,23-25] as well as spectroscopic ellipsometry (SE) measurements. SE has received an increasing attention in recent years [26] as a fast, reliable and highly sensitive method for measuring optical properties of thin film materials. Using polarized light as the probe, SE measures the change in polarization state of light reflected from (or transmitted through) the surface of a sample over a wide spectral window, providing several unique advantages as compared to the T/R measurement [27]. Firstly, two parameters ( $\Psi$  and  $\Delta$ ) instead of one are independently determined in a single-measurement at each wavelength. Therefore, both the real and imaginary parts of the complex dielectric function can be obtained directly on a wavelength-by-wavelength basis without having to resort to multiple measurements or to performing the Kramers-Kronig analysis. Secondly, SE measurement is highly surface sensitive and can be used to measure film down to sub-monolayer thickness. The variable angle measurement allows acquiring a large amount of data and minimizing parameter correlations in the model fitting. Finally, SE measures the reflected intensity with reference to the incident light, and hence no special reference sample is needed and results are not affected by fluctuations in the source intensity.

Optical properties of common TCOs such ITO and AZO have been studied by SE [5, 19, 28]. The effects of free carriers on the optical response of doped TCO thin films were found to be significant, in both the infrared (IR) and the band-edge region. It has been shown that in Al-doped ZnO thin films with carrier density of  $1 \times 10^{21} \text{ cm}^{-3}$  the free carrier plasma contribution to the dielectric function in the IR region screens the polar lattice mode excitation, and results in a Burstein-Moss effect related blueshift of the optical absorption edge [5]. Similar effects should be observed for high carrier concentration, intentionally doped CdO thin films. However, to date only a few SE investigations on CdO have been reported [8]. In this work, we report a comprehensive study of optical properties of CdO thin films doped with two different types of dopants: shallow donors (In and Ga) and transition metals (V and Ti) with electron concentration as high as  $2 \times 10^{21} / \text{cm}^3$  using variable angle spectroscopic ellipsometry (VASE) in the spectral range of 190 to 1700 nm (0.73 to 6.5 eV). Moreover, the electron effective mass for films with different dopants was derived from SE and Hall Effect measurements.

## 2. EXPERIMENT

CdO thin film samples were deposited using a dual-gun radio frequency magnetron sputtering system. In, Ga, Ti and V doping was achieved by using a  $\text{In}_2\text{O}_3$ ,  $\text{Ga}_2\text{O}_3$ ,  $\text{TiO}_2$  and  $\text{V}_2\text{O}_3$  target, respectively sputtered together with a CdO target. Some of the In doped CdO films were also deposited using a 2% and 4% In doped

CdO sintered target. The dopant concentration was tuned by varying the sputtering power and the substrate-target distance of dopant targets. Both soda lime glass and silicon substrates were used with substrate temperature maintained at 270°C during deposition. Prior to deposition, the chamber was pumped down to  $\sim 1 \times 10^{-6}$  Torr, and the background pressure was maintained at 5 mTorr by flowing pure Ar or Ar mixed with O<sub>2</sub> (1~2%) during deposition.

Film stoichiometry, dopant concentration and thickness were measured by Rutherford backscattering (RBS) using a 3.04 MeV He<sup>++</sup> beam. Film thicknesses in the range of 100-350 nm were measured by RBS and also confirmed by SE. The crystalline structure of films was determined by x-ray diffraction (XRD). Typically polycrystalline films with grain size in the range of 10-24 nm were synthesized. Carrier concentration and Hall mobility were obtained from Hall measurement in the van der Pauw configuration. Room temperature SE spectra (the amplitude ratio  $\psi$ , and the phase difference  $\Delta$ ) were measured in the spectral range of 0.73 to 6.5 eV using a rotating-compensator instrument (J. A. Woollam, M-2000). The angle of incidence was varied from 60° to 75° with an increment of 5°. The back side of the glass substrate was taped with translucent plastic tape to eliminate back-side reflection [29]. The rotating compensator ellipsometer provides accurate results for the ellipsometric parameters  $\psi$  and  $\Delta$  over the complete measurement range ( $\psi=0-90^\circ$ ,  $\Delta=0-360^\circ$ ). This is a clear advantage over the commonly used rotating-analyzer (polarizer) ellipsometer whose measurement errors increase significantly when  $\Delta$  approaches to 0° and 180° [19,30].

### 3. SE ANALYSIS

SE data analysis was carried out using a 3 layer structure, including a surface roughness layer, CdO film and glass substrate. The refractive index ( $n$ ) of the glass substrate was determined by fitting the ellipsometric parameter  $\psi$  while the extinction coefficient ( $k$ ) was obtained by fitting the normal incidence transmission spectrum on a bare glass substrate, according to the procedure outlined in the WVASE32® [31]. The dielectric function of the surface roughness layer was modeled as a 50/50 vol% mixture of the CdO bulk layer and voids [32]. The optical response of free electrons in metal or metal-like materials is typically described by the Drude model [19, 31], while for TCO materials, a variety of models including Lorentz model, Tauc-Lorentz (TL) model and the Cauchy model have been used to account for contributions from interband optical transitions. Here for highly conducting CdO thin films the Drude model combined with the Tauc-Lorentz model is used to describe the dielectric function  $\epsilon(E)$  as

$$\epsilon(E) = \epsilon_1(E) - i\epsilon_2(E) = \epsilon_D(E) + \epsilon_{TL}(E), \quad (1)$$

where  $\epsilon_D(E)$  and  $\epsilon_{TL}(E)$  are the dielectric functions calculated by the Drude and TL models, respectively.  $\epsilon_D(E)$  describes the intraband while  $\epsilon_{TL}(E)$  accounts for the interband optical transitions in the film. This combined model has been used successfully to fit the SE data of SnO<sub>2</sub>:F, ZnO:Ga and In<sub>2</sub>O<sub>3</sub>:Sn films [19, 33,34].  $\epsilon_D(E)$  is given by

$$\varepsilon_D(E) = -\frac{A_D}{E^2 - i\Gamma_D E}, \quad (2)$$

where the two parameters ( $A_D$ ,  $\Gamma_D$ ) represent the amplitude and the broadening, respectively. Based on the Drude theory, the amplitude  $A_D$  can be expressed as

$$A_D = \varepsilon_\infty E_p^2, \quad (3)$$

where  $\varepsilon_\infty$  and  $E_p$  are the high-frequency dielectric constant and plasma energy, respectively. The plasma energy, in turn can be written as

$$E_p = \hbar\omega_p = \sqrt{\frac{\hbar^2 e^2 N_{opt}}{m^* \varepsilon_\infty \varepsilon_o}}. \quad (4)$$

In Eq. (4)  $\omega_p$ ,  $e$ ,  $N_{opt}$  and  $\varepsilon_o$  are the plasma angular frequency, electron charge, optical carrier concentration, and the free-space permittivity, respectively. The broadening parameter in the Drude model is related with the electron effective mass ( $m^*$ ) and the optical mobility ( $\mu_{opt}$ ) by

$$\Gamma_D = \frac{\hbar e}{m^* \mu_{opt}}. \quad (5)$$

At sufficiently low energies, the real part of dielectric function  $\varepsilon_1(E)$  can be written as

$$\varepsilon_1(E) = \varepsilon_\infty - \frac{A_D}{E^2 + \Gamma_D^2}. \quad (6)$$

Hence  $\varepsilon_\infty$  can be obtained from the intercept of  $\varepsilon_1(E)$  plotted against  $1/(E^2 + \Gamma_D^2)$ , [19,35,36].

In the TL model  $\varepsilon_{TL}(E) = \varepsilon_{TL1} + i\varepsilon_{TL2}$ , where

$$\varepsilon_{TL2} = \left[ \frac{A_{TL} E_o C (E - E_T)^2}{(E^2 - E_o^2)^2 + C^2 E^2} \times \frac{1}{E} \right] \text{ for } E > E_T, \quad (7)$$

$$\varepsilon_{TL2} = 0 \text{ for } E < E_T. \quad (8)$$

The  $\varepsilon_{TL1}$  obtained by Kramers-Kronig relation and integration is given by

$$\varepsilon_{TL1}(E) = \varepsilon_1(\infty) + \frac{2}{\pi} P \int_{E_T}^{\infty} \frac{\xi \varepsilon_{TL2}(\xi)}{\xi^2 - E^2} d\xi, \quad (9)$$

with  $P$  being the Cauchy principal part of the integral [37]. Thus, in the TL model, the dielectric function is described by five parameters  $\{A_{TL}, E_o, C, E_T, \varepsilon_1(\infty)\}$  which represent the amplitude, center energy, broadening, Tauc optical gap, and energy-independent contribution to real part of dielectric function, respectively. Therefore, the various optical and electronic properties such as  $\varepsilon_\infty, E_p, N_{opt}, \mu_{opt}$ , and  $m^*$  can be derived from the experimentally determined dielectric function.

## 4. RESULTS AND DISCUSSTION

### 4.1 Electrical properties

The electrical properties of CdO films doped with In, Ga, V and Ti with various doping concentration (given in mole percent) obtained by Hall effect measurements are summarized in Fig. 1. All the dopant species studied in this work are efficient donors in CdO and as shown in Fig. 1(a) electron concentration  $N$  increases to  $>10^{21}/\text{cm}^3$  with dopant concentration up to 6-10 mole fraction (or  $2.3\text{-}3.8 \times 10^{21}/\text{cm}^3$ ). However, as is seen in Fig. 1 (b) there is a significant difference in the electron mobility behavior between group III shallow donors (Ga and In) and transition metal (V and Ti) dopants. While high mobility of  $\sim 130 \text{ cm}^2/\text{Vs}$  can be achieved for doping with group III donors for  $n \sim 10^{21}/\text{cm}^3$ , doping with transition metals (TMs) results in a rapid drop in the mobility from 90 to  $<10 \text{ cm}^2/\text{Vs}$  at high electron concentrations. The dramatic difference in the mobility behavior can be attributed to the different doping mechanisms of the two types of dopants. Column III Ga and In substituting Cd site contribute two electrons to the bonds and the third loosely bound electron falls into the conduction band and is responsible for the n-type conductivity in CdO. On the other hand, group 3d TM substituting Cd contribute two outer 4s electrons to the bonds and their electrical activity depends on the location of the donor or acceptor level associated with the 3d band. Thus, as has been shown before, the energy of the donor d-levels of V and Ti are located at  $\sim 5.0$  and  $4.8 \text{ eV}$  below the vacuum level, respectively [38] placing these levels at about  $1 \text{ eV}$  above the CdO conduction band edge located at  $\sim 5.8 \text{ eV}$ . Consequently both V and Ti provide free electrons to the conduction band of CdO until the Fermi level reaches the localized d-level energy. The electronic structure parameters derived from an analysis of the spectroscopic ellipsometry measurements will help us to better understand these different doping mechanisms.

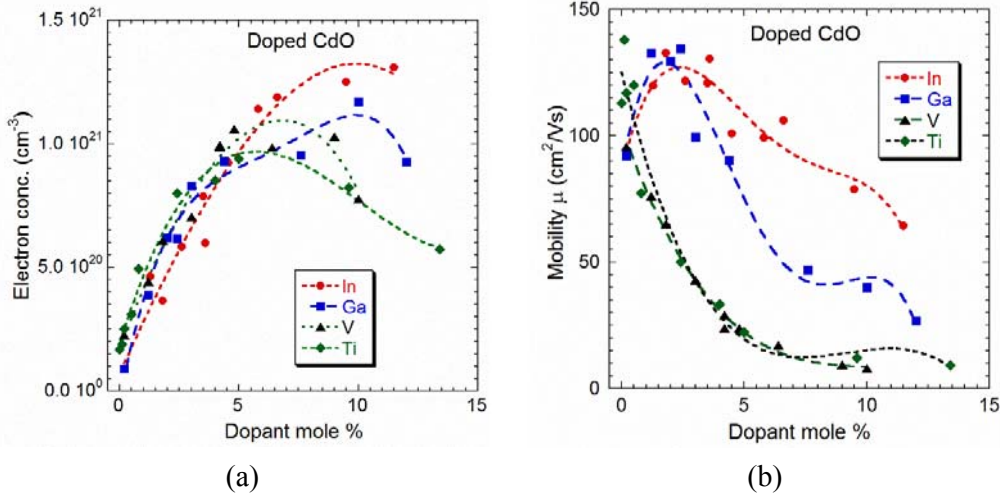


Fig. 1. Electron concentration (a) and mobility (b) for CdO films doped with group III (Ga and In) and transition metal (V and Ti) dopants with increasing dopant concentration. The dash lines are guides to the eyes using simple polynomial fitting of data points.

#### 4.2 Complex dielectric functions

Fig. 2 shows the measured (black dotted line) SE spectra of a In doped CdO (CdO:In) thin film with Hall electron concentration ( $N_{\text{Hall}}$ ) of  $6.6 \times 10^{20} \text{ cm}^{-3}$ . We found that, as is shown in Fig.2, the adopted dielectric function model (solid curve) can fit the experimental SE data very well if the energy range is confined to lower than  $3.5$

eV. This is understandable as our simple model cannot be used to describe the optical function at energies much higher than the band gap [19]. Nevertheless, optical response with photon energy up to 3.5 eV is sufficient for us to investigate the free carrier effects in CdO thin films with band edge absorption at energy less than 3.5 eV. The corresponding fitting parameters for SE data shown in Fig. 2 are given in table I.

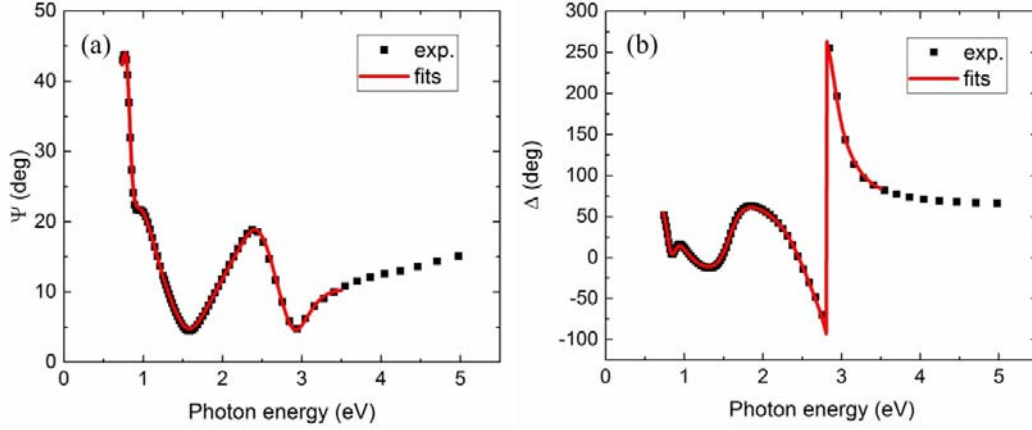


Fig. 2: The measured (black square) and the fitted (red solid line) SE spectra of CdO:In thin film, with  $N_{Hall}=6.6 \times 10^{20} \text{ cm}^{-3}$  and angle of incidence of  $70^\circ$ .

Table I: The fitting parameters extracted from the dielectric function modeling using the Drude model and Tauc-Lorentz model for CdO:In thin film on glass substrate, with  $N_{Hall} = 6.6 \times 10^{20} \text{ cm}^{-3}$ . The dopant (In) concentration in the film is around 4%.

CdO: In ( $N_{Hall}=6.6 \times 10^{20} \text{ cm}^{-3}$ )	
$d_s$ (nm)	$5.208 \pm 0.084$
$d_f$ (nm)	$119.22 \pm 0.09$
$A_D$	$3.0256 \pm 0.0040$
$\Gamma_D$	$0.0588 \pm 0.0003$
$A_{TL}$ (eV)	$221.5 \pm 16.0$
$C$ (eV)	$7.751 \pm 0.246$
$E_T$ (eV)	$2.584 \pm 0.008$
$E_0$ (eV)	$3.990 \pm 0.168$
$\epsilon_l(\infty)$	1 (fixed)
MSE	19.4

The complex dielectric function and the complex refractive index of CdO:In thin films with different  $N_{Hall}$  are shown in Fig. 3. As seen from the imaginary part of dielectric function ( $\epsilon_2$ ) or the extinction coefficient ( $k$ ), significant free carrier absorption in the NIR region is observed with high  $N_{Hall}$ . The plasma energy ( $E_p$ ) can be extracted at the photon energy where  $\epsilon_1(E) = 0$ . Due to the limited IR energy range for the SE measurement, the  $E_p$  could not be obtained for thin films with electron concentration lower than  $5 \times 10^{20} \text{ cm}^{-3}$ . As seen in Fig. 3b, the refractive index ( $n$ ) increases with the photon energy, with a trend similar to that found in other



TCOs [39]. For CdO thin film with extremely high carrier concentration the refractive index drops drastically at low energy (e.g.,  $<1$  eV or  $\lambda > 1200$  nm). Furthermore, as is seen in Fig. 3b  $n$  of CdO:In films decreases from with increasing  $N_{Hall}$ , e.g. at photon energy of 2 eV  $n$  decreases from 2.3 to 2 as  $N_{Hall}$  increases from  $2.3 \times 10^{20}$  to  $1.18 \times 10^{21}/\text{cm}^3$ .

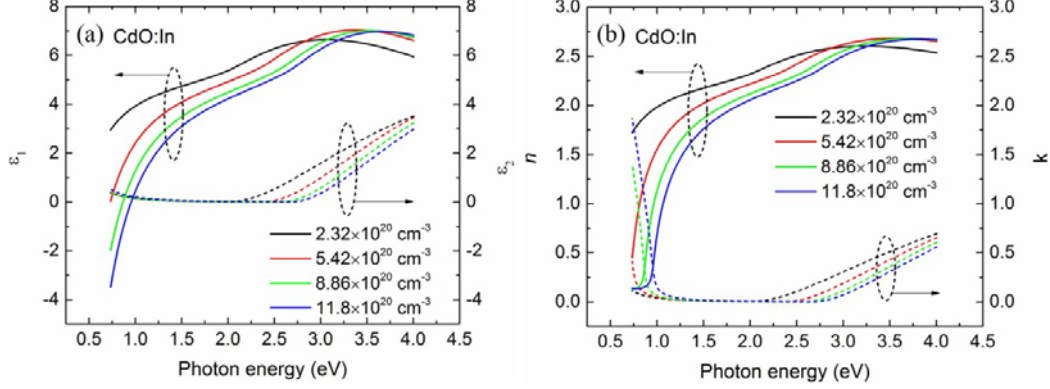


Fig. 3: (Color online) the complex dielectric function (a) and the complex refractive index (b) extracted from the optical model for CdO:In thin films with variable  $N_{Hall}$ .

#### 4.3 Free carrier absorption and refractive index

In order to get more accurate dielectric functions in a wide spectral range we fitted the SE data by using a more elaborate dielectric function model in which we added two more Gaussian oscillators to the Drude model and combined it with the TL model. The extracted complex dielectric functions of CdO thin films with  $N_{Hall} \sim 8 \times 10^{20} \text{ cm}^{-3}$  doped with different dopants as well as that of a typical undoped CdO thin film with  $N_{Hall} = 1.29 \times 10^{20} \text{ cm}^{-3}$  are shown in Fig. 4a. It worth noting that the obtained dielectric function of undoped CdO thin film is rather close to that of single crystalline CdO film with similar carrier concentration ( $N_{Hall} = 2 \times 10^{20} \text{ cm}^{-3}$ ), as reported by Choi et al. [8]. Absorption coefficients of these samples derived from the dielectric functions are shown in Fig. 4b. As expected the absorption edge of doped CdO sample with high  $N_{Hall}$  blue-shifts due to Burstein-Moss effect. At the same time, free carrier absorption,  $\alpha_{FCA}$  becomes significant in the low energy region  $0.74 < E < 1$  eV for the films with high carrier concentration. It is interesting to note that as is shown in the inset of Fig. 4(b) the low photon energy absorption coefficient  $\alpha$  is dependent on the dopant species. Thus with similar  $N_{Hall}$  of  $\sim 8 \times 10^{20} \text{ cm}^{-3}$ ,  $\alpha$  is larger in the TM doped than In or Ga doped films for  $E > 0.9$  eV and smaller for  $E < 0.8$  eV.

Based on the Drude model,  $\alpha_{FCA}$  are given by  $Ne^2/(\epsilon_0 cn \mu (m^* \omega)^2)$ , with  $N$  being the free carrier concentration,  $e$  the electron charge,  $\epsilon_0$  the permittivity in free space,  $c$  the speed of light in vacuum,  $n$  the refractive index of material,  $\mu$  the carrier mobility,  $m^*$  the electron effective mass, and  $\omega$  the photon angular frequency [18]. The dotted lines in the inset of Fig. 4b were calculated using the effective mass and the optical mobility derived from eq. (4) and eq. (5) (discussed in the following sections) for the doped samples, while for the undoped thin film,  $m^* = 0.23m_e$  and

$\mu = 84 \text{ cm}^2/\text{Vs}$  (Hall mobility) were assumed. The calculated  $\alpha_{\text{FCA}}$  agree well with  $\alpha$  at relatively low energy, indicating that  $\alpha_{\text{FCA}}$  dominates the absorption at low energies. Since  $\alpha_{\text{FCA}} \propto N/\mu$ , the higher  $\alpha_{\text{FCA}}$  of TM doped CdO thin films at  $E > 0.8 \text{ eV}$  is mainly attributed to their lower carrier mobility; while the lower  $\alpha_{\text{FCA}}$  at energy  $E < 0.8 \text{ eV}$  for the TM doped CdO is due to their much larger refractive index (e.g.,  $n \sim 0.7$  for CdO:V and  $n \sim 0.13$  for CdO:In).

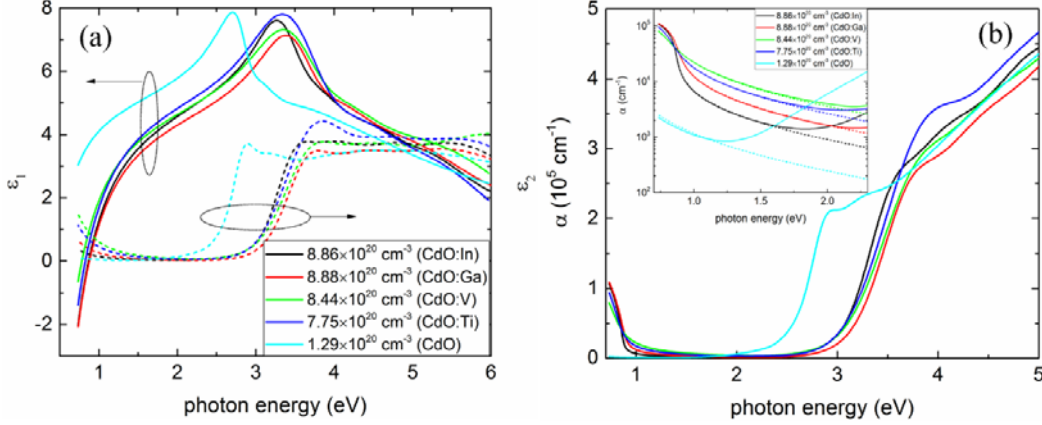


Fig. 4: (Color online) the complex dielectric function of doped (In, Ga, V, Ti) CdO thin film with similar  $N_{\text{Hall}}$  (a), and the absorption coefficient of the doped CdO thin films (b). The inset in (b) is the corresponding  $\alpha$  in a smaller energy range (0.74~2.3 eV) in the log scale, with the dotted lines representing the calculated  $\alpha_{\text{FCA}}$ . The undoped CdO thin film with  $N_{\text{Hall}} \sim 1.29 \times 10^{20} \text{ cm}^{-3}$  is also shown for comparison.

The dependence of free carrier absorption in the NIR region at wavelength of 1200 nm and the refractive index ( $n$ ) in the visible region at 600 nm on the  $N_{\text{Hall}}$  are shown in Fig. 5a and 5b, respectively. Fig. 5a shows that for all dopants  $\alpha(\lambda = 1200 \text{ nm})$  generally increases with  $N_{\text{Hall}}$  and then tends to saturate at high electron concentration for all dopants. Specifically,  $\alpha$  increases from  $10^2 \text{ cm}^{-1}$  to  $1 \times 10^4 \text{ cm}^{-1}$  as  $N_{\text{Hall}}$  increases from  $2 \times 10^{20} \text{ cm}^{-3}$  to  $12 \times 10^{20} \text{ cm}^{-3}$ . We note that for  $N_{\text{Hall}} > 5 \times 10^{20} \text{ cm}^{-3}$  doping with In or Ga results in over 2 to 3 times lower absorption compared with the samples doped with TMs. As mentioned earlier, this difference in  $\alpha$  is attributed to the low mobility of TM doped materials [7].

As is seen in Fig. 5b the refractive index of doped CdO thin film taken at  $\lambda = 600 \text{ nm}$  is monotonously decreasing with increasing  $N_{\text{Hall}}$ . Unlike the absorption coefficient, the refractive index  $n(\lambda = 600 \text{ nm})$  does not show any discernable dependence on the different dopant species. Carrier-induced change in refractive index is related to the change in absorption coefficient  $\Delta\alpha$ , given by

$$\Delta n(E) = \frac{2ch}{e^2} P \int_0^\infty \frac{\Delta\alpha(E')}{E'^2 - E^2} dE', \quad (10)$$

where  $c$  is the speed of light,  $e$  is the electron charge,  $E$  is the photon energy, and  $P$  indicates the principal value of the integral [40]. The free carrier induced change of the absorption coefficient  $\Delta\alpha$  is caused by three different effects: Burstein-Moss shift, band gap renormalization, and the free carrier absorption effect. In the Drude model,

the intraband free carrier absorption induced change in the refractive index is given by  $\Delta n = -\frac{e^2 \lambda^2 N}{8\pi^2 c^2 \epsilon_0 n m^*}$ , where the  $N$  is the electron concentration [40]. The linear decrease in  $n(\lambda = 600\text{nm})$  of doped CdO thin film most likely related to the fact that both free carrier absorption and the Burstein-Moss effect induced change in the refractive index linearly depend on the free carrier concentration [40]. Note that the refractive index of doped or undoped CdO thin film with low carrier concentration  $N_{Hall} < 3 \times 10^{20} \text{ cm}^{-3}$  is equal to  $\sim 2.3$  at 600 nm. This is close to the value reported for epitaxial CdO film with  $N_{Hall}$  of  $2 \times 10^{20} \text{ cm}^{-3}$  [8]. The refractive index of TCO is an important parameter in optical design for optoelectronic devices, *e.g.*, in solar cell device where the TCO serves as the front electrode, and could be as an anti-reflection coating [41]. For instance, for silicon solar cell with  $n \sim 3.9$  at 600 nm the minimum light reflection is achieved for TCO with  $n = 2.4$ , which is very close to that of CdO thin films.

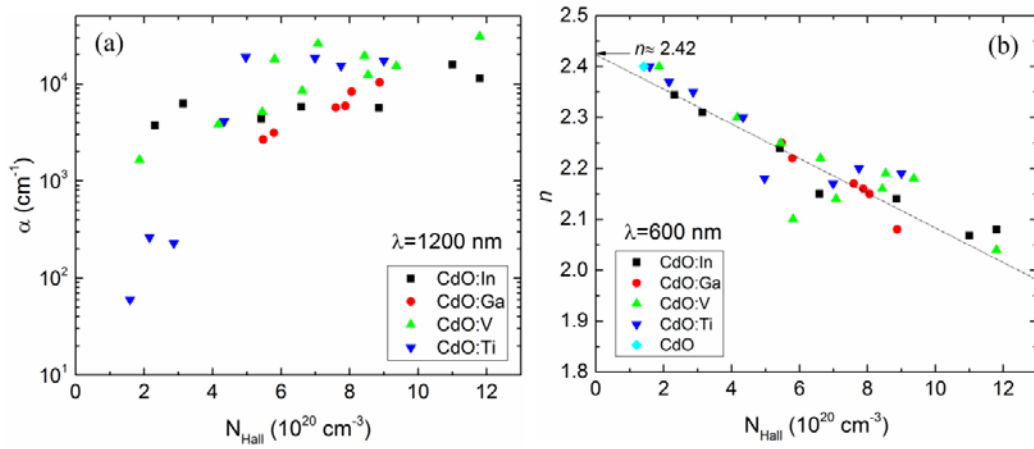


Fig. 5: (Color online) absorption coefficient (a) at wavelength of 1200 nm and the refractive index (b) at wavelength of 600 nm of CdO thin films doped with various dopants (In, Ga, V, Ti) obtained from SE analysis. The refractive index of undoped CdO thin film is also given for reference.

#### 4.4 High frequency dielectric constant

Fig. 6a shows plots of  $\epsilon_2$  of CdO:In thin films with different  $N_{Hall}$  as a function of  $1/(E^2 + \Gamma_D^2)$ . As indicated in Eq. (6), the high frequency dielectric constant  $\epsilon_\infty$  can be obtained from the x-intercept of these plots. Values of  $\epsilon_\infty$  for CdO doped with different dopants (In, Ga, V, Ti) are plotted as a function of  $N_{Hall}$  in Fig. 6b. We observe that the  $\epsilon_\infty$  of CdO decreases roughly linearly from  $\sim 5.5$  to 4.9 with increasing  $N_{Hall}$  with no obvious dependence of the dopant species. Such linear dependence of  $\epsilon_\infty$  on carrier concentration was also found for other TCOs, *e.g.*, ZnO:Ga and  $\text{In}_2\text{O}_3$ :Sn [19]. The  $\epsilon_\infty$  values of CdO thin films with different carrier concentration obtained from SE measurements are close to that reported by H. Finkenrath *et al.* [42] and are much higher than those of other conventional TCOs. For CdO, ITO and GZO with electron concentration  $N = 10^{21}/\text{cm}^3$ , the respective values of  $\epsilon_\infty$  are 5.0, 4.05 and 3.6 for [19].

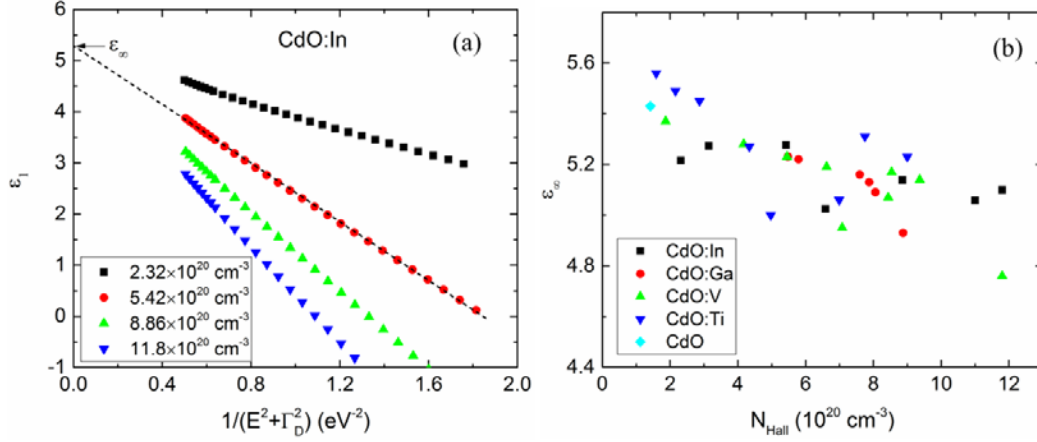


Fig. 6: (Color online) The real part of dielectric function  $\epsilon_1$  (a) plotted as function of  $1/(E^2 + \Gamma_D^2)$ , and the high frequency dielectric constant (b) of CdO thin films with dependence on Hall carrier concentration.

The values of plasma wavelength  $\lambda_p$  obtained from Eq. (4) for doped CdO thin films are shown in Fig. 7. The  $\lambda_p$  of In or Ga doped CdO thin film with variable carrier concentration is consistent with our previous work, in which the  $\lambda_p$  was obtained by fitting the experimental reflectance spectrum using a constant effective mass of  $0.2m_o$  [7]. In contrast  $\lambda_p$  of TM doped CdO films are much larger. This can be attributed to the enhancement of the electron effective mass by TM doping (see Eq. 4). As is seen in Fig. 7  $\lambda_p$  values for ITO, AZO and GZO adopted from the literature are consistently smaller than that of CdO. The higher  $\lambda_p$  for CdO broadens the transparency window and makes this material particularly suited for transparent conductor applications in the IR regime.

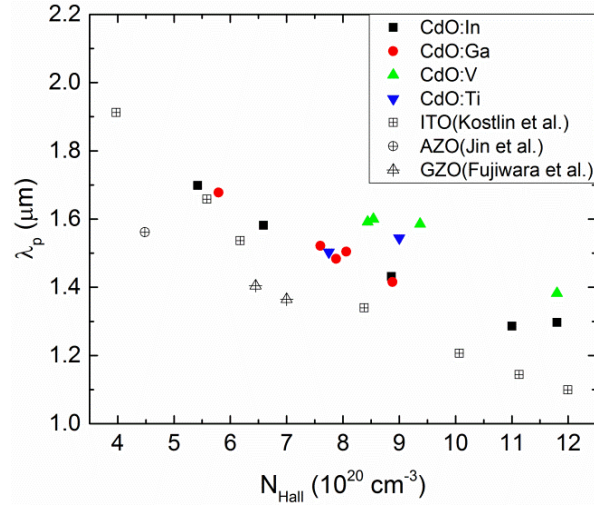


Fig. 7: The plasma wavelength obtained from SE analysis for doped CdO thin films as a function of  $N_{\text{Hall}}$ . The previously reported results for other TCOs by Kostlin *et al.* (Ref.43), Jin *et al.* (Ref.44), and Fujiwara *et al.* (Ref. 19) are also shown for comparison.

#### 4.5 Electron effective mass

Using the values of  $\varepsilon_\infty$  shown in Fig. 6b and assuming  $N_{opt} = N_{Hall}$  one can calculate the electron effective mass  $m^*$  of CdO from Eq. (4). The results in Fig. 8 show that the effective mass is nonlinearly increasing with  $N_{Hall}$ . In addition, a rapid increase of the effective mass is observed in TM doped CdO at  $N_{Hall} > 8 \times 10^{20} \text{cm}^{-3}$ . The dependence of  $m^*$  on electron concentration in In and Ga doped samples can be explained by a nonparabolicity of the conduction band of CdO in a way similar to that used for other TCOs [45,46]

$$m^* = m_o^* \sqrt{1 + 2C \frac{\hbar^2}{m_o^*} (3\pi^2 N)^{\frac{2}{3}}}, \quad (11)$$

where  $m_o^*$  is the effective mass at the bottom of the conduction band,  $C$  is a nonparabolicity parameter,  $N$  is the carrier concentration and is taken as  $N_{Hall}$  here. The black solid line shown in Fig. 8 is the best fit of the effective mass data for the In and Ga doped CdO samples with  $m_o^*$  and  $C$  as fitting parameters. The best fit results for  $m_o^*$  and  $C$  are  $0.13 \pm 0.04 m_o$  and  $0.5 \pm 0.2 \text{ eV}^{-1}$ , respectively. Here  $m_o$  is the free electron mass. Fits with  $m_o^*$  fixed at  $0.1$  and  $0.2 m_o$  (dash lines) are also shown for comparison. In our previous work [7] a higher band edge effective mass  $m_o^* = 0.2 m_o$  was assumed. However, Fig. 8 shows that a reasonable fit of our data cannot be obtained by assuming a  $m_o^* = 0.2 m_o$ . Note that  $m_o^*$  ranging from  $0.12$  to  $0.2$  has been reported [17, 47-49]. Unlike most reports where the effective mass was obtained by assuming a constant high frequency dielectric constant  $\varepsilon_\infty$ , the  $m^*$  in Fig. 8 were calculated using the carrier concentration dependent  $\varepsilon_\infty$  in Fig. 6b. The nonparabolicity parameter  $C$  of CdO obtained in this work is very close to that reported for ITO ( $C \sim 0.5 \text{ eV}^{-1}$ ) by Feneberg *et al.*, [28] but much higher than that of GZO ( $C \sim 0.142 \text{ eV}^{-1}$ ) reported by Fujiwara *et al.* [19] Table II shows a comparison of various parameters of In and Ga doped CdO with the literature values of these parameters for ITO and GZO.

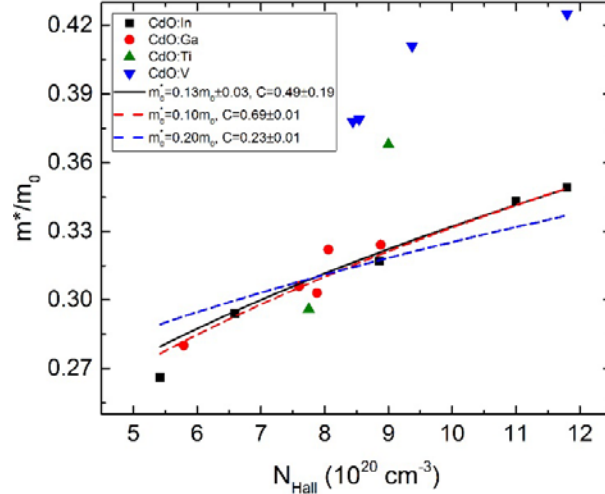


Fig. 8: Electron effective mass  $m^*$  for CdO thin films with different dopants as a function of  $N_{Hall}$ , where  $m_o$  is the free electron mass. The black line is the best fit for data from the In and Ga doped samples by using Eq. (11), the dashed lines are fits with fixed  $m_o^*$  with values of  $0.1$  and  $0.2 m_o$ .

The much higher effective mass obtained for the TM doped CdO is related to the presence of partially occupied d states of the dopant species. Garcia-Hemme et al. have shown by optical absorption and photoluminescence measurements that the anticrossing interaction between the localized d-levels of V atoms and the extended states of the ZnO CB results in an upward shift of the mostly unoccupied conduction band states ( $E_+$  sub-band) and broadening of the occupied V donor d-levels into a narrow band ( $E_-$  sub-band) [54]. Such anticrossing interaction also occurs in the TM doped CdO resulting in a modification of the conduction band dispersion relation. The flattening of the dispersion relation for the  $E_-$  subband is reflected in an increase in the electron effective mass.

Table II. A comparison of parameters of CdO obtained from SE measurements and those for ITO and GZO/AZO from the literature.

	CdO (this work)	ITO	GZO/AZO
$n$ ( $\lambda=600\text{nm}$ ) ( $N=7 \times 10^{20}/\text{cm}^3$ )	2.2	1.8 [19, 50] ~1.9 [53]	1.7 [19,GZO]
$\epsilon_\infty(N=0)$	5.4	4.62 [19]	3.9 [19,GZO]
$\epsilon_\infty$ ( $N=1 \times 10^{21}/\text{cm}^3$ )	5.0	4.05 [17], ~3.0 [53] <3.0 [50]	3.6 [19,GZO]
$C$ ( $\text{eV}^{-1}$ )	0.5	0.18 [19], 0.5 [28]	0.142 [19,GZO]
$m_o^*/m_o$	0.13	0.3 [19] 0.18 [28]	0.28 [19,GZO] 0.30 [51 ,GZO]
$m^*$ ( $N=1 \times 10^{21}/\text{cm}^3$ )	0.33	0.407 [19] 0.4 [28], ~0.38 [53]	0.38 [19,GZO] 0.43 [52, AZO]

#### 4.6 Optical band gap

The absorption coefficient ( $\alpha$ ) can be calculated from the measured extinction coefficient,  $k$  using the equation  $\alpha=4\pi k/\lambda$ . Assuming the transition probability becomes constant at the absorption edge, the absorption coefficient for the direct allowed transition can be estimated as  $\alpha \approx (E - E_G^{opt})^{1/2}$  [55]. The optical band gap  $E_G^{opt}$  can then be estimated by extrapolating  $\alpha^2$  to zero photon energy. Fig. 9a shows  $\alpha^2(E)$  plots for CdO:In films with different  $N_{Hall}$  and the  $E_G^{opt}$  obtained are plotted in Fig. 9b. Since highly conducting TCOs are typically degenerately doped, the optical band gap  $E_G^{opt}$  are larger than its intrinsic band gap due to Burstein-Moss effect and band gap renormalization. [56,57].

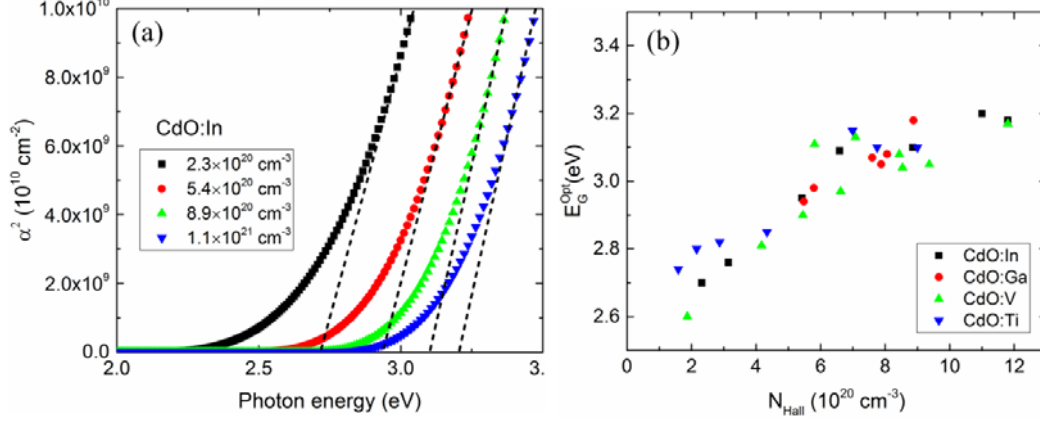


Fig. 9: Plotting of  $\alpha^2$  as a function of photon energy for CdO:In films with different  $N_{Hall}$  (a), and optical band gap of doped CdO thin films as a function of  $N_{Hall}$  (b).

The optical band gap of a heavily doped n-type semiconductor can be expressed as

$$E_G^{Opt} = E_G + \Delta E_G^{BM} - \Delta E^{BGN}, \quad (12)$$

where  $E_G$ ,  $\Delta E_G^{BM}$ ,  $\Delta E^{BGN}$  are the intrinsic band gap, the Burstein-Moss shift, and the band gap renormalization, respectively [56-58]. In this work, the  $\Delta E_G^{BM}$  was calculated by using the nonparabolic conduction band model [45], while the band gap renormalization was evaluated by Jain's model [59,60],

$$\frac{\Delta E^{BGN}}{R} = \frac{1.83}{r_s} \frac{\Lambda}{N_b^{1/3}} + \frac{0.95}{r_s^{3/4}} + \frac{\pi}{2} \frac{1}{r_s^{3/4} N_b} \left( 1 + \frac{m_{min}^*}{m_{maj}^*} \right), \quad (13)$$

where  $R$  is the effective Rydberge energy,  $N_b$  is the number of equivalent band extrema,  $\Lambda$  is the correction factor accounting for anisotropy of bands in n-type semiconductors and interaction between the heavy-and light-hole bands in p-type semiconductors,  $r_s$  is the average distance (normalized to the effective Bohr radius) between majority carriers,  $m_{min}^*$  and  $m_{maj}^*$  are minority and majority carrier density of state effective masses, respectively. The parameter values used for calculating  $\Delta E^{BGN}$  by Eq. (13) is adopted from work by Zhu *et al* [58]. Fig. 10 shows the band gap shift ( $E_G^{Opt} - E_G$ ) for doped CdO thin films as a function of  $N_{Hall}$ . Here the intrinsic band gap  $E_G$  of 2.3 eV for CdO is used. The calculated  $\Delta E_G^{BM}$ ,  $\Delta E^{BGN}$ , and  $\Delta E_G^{BM} - \Delta E^{BGN}$  are also shown for comparison. We found that band gap shift ( $E_G^{Opt} - E_G$ ) for the doped CdO thin films agrees well with the calculated values and the apparent shifts are independent of the dopant species.



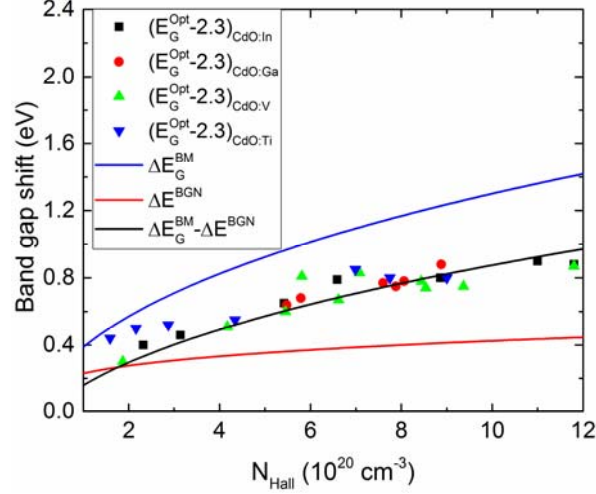


Fig. 10: (Color online) Band gap shift of doped CdO thin films as a function of  $N_{Hall}$ , assuming an intrinsic band gap of 2.3 eV. The calculated Burstein-Moss shift  $\Delta E_G^{BM}$ , the band gap renormalization  $\Delta E_G^{BGN}$ , as well as  $\Delta E_G^{BM} - \Delta E_G^{BGN}$  are also illustrated.

#### 4.7 Optical mobility

The optical mobility  $\mu_{opt}$  was determined from the experimentally measured broadening parameter  $\Gamma_D$  using Eq. 5. Fig. 11a compares  $\mu_{opt}$  of doped CdO films with the mobility measured by Hall effect  $\mu_{Hall}$ . The effective mass shown in Fig. 8 was used in the calculation. The dotted line in Fig. 11a indicates the case when  $\mu_{opt} = \mu_{Hall}$ . As shown in Fig. 11a,  $\mu_{opt}$  is very close to  $\mu_{Hall}$  when  $\mu_{Hall} < 60 \text{ cm}^2/\text{Vs}$ . However, for doped CdO films with  $\mu_{Hall} > 60 \text{ cm}^2/\text{Vs}$ , we found that  $\mu_{opt} < \mu_{Hall}$ . It has been argued that the  $\mu_{opt}$  represents an average intra-grain mobility of polycrystalline materials and is generally higher than  $\mu_{Hall}$  since  $\mu_{Hall}$  represents the average mobility of electrons undergoing multiple grain boundary scattering [17].  $\mu_{Hall} \geq \mu_{opt}$  suggests that the mobility of CdO is not affected by grain boundaries scattering. This is consistent with the high electron affinity (5.8 eV) of CdO which gives rise to electron accumulation at CdO grain boundaries.

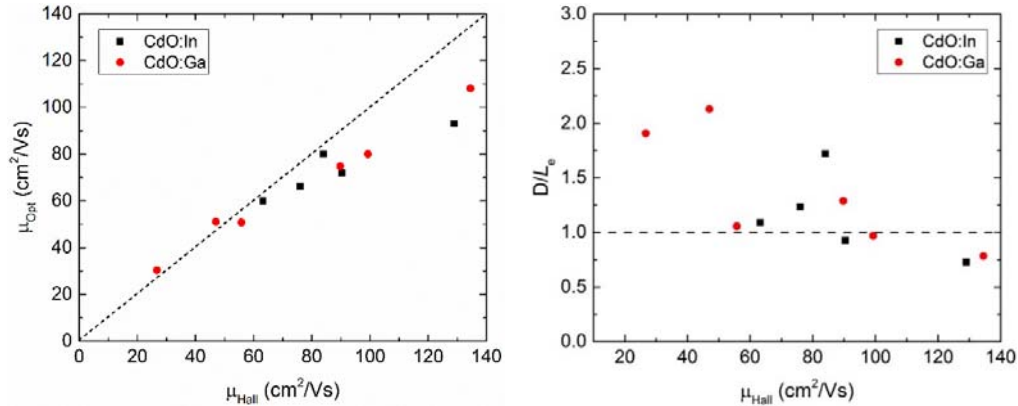


Fig. 11: (a) Optical mobility ( $\mu_{opt}$ ) obtained from SE analysis using the effective mass



presented in Fig. 8, and (b) mean free path of CdO thin films as a function of  $\mu_{\text{Hall}}$ .

Based on the degenerate electron gas model, the mean free path of electrons is given by

$$L_e = (3\pi^2)^{\frac{1}{3}} \left( \frac{\hbar}{e^2} \right) \rho^{-1} N^{-\frac{2}{3}}, \quad (14)$$

where  $\rho$  and the  $N$  are the resistivity and the carrier concentration, respectively [61,62]. The average grain size ( $D$ ) of CdO films estimated from XRD measurements is  $\sim 10$ -25 nm. Fig. 11b shows a plot of  $D/L_e$  as a function of  $\mu_{\text{Hall}}$  for the In and Ga doped CdO. We found that for films with high mobility, which has  $\mu_{\text{Hall}} \geq \mu_{\text{opt}}$ , the grain size is comparable or smaller than the electron mean free path ( $D/L_e \leq 1$ ). This again suggests that the effect of grain boundary scattering on the  $\mu_{\text{Hall}}$  is negligible in these films.

Although cases with  $\mu_{\text{opt}} < \mu_{\text{Hall}}$  were also previously reported for  $\text{In}_2\text{O}_3:\text{Sn}$  [19],  $\text{SnO}_2:\text{F}$  [63], and  $\text{CdO}:\text{In}$  films grown by cathodic arc deposition [17], there is no clear explanation on this phenomenon. Mendelsberg *et al.* suggested that electrons crossing the grain boundaries during the optical excitation may bring  $\mu_{\text{opt}}$  closer to  $\mu_{\text{Hall}}$  for films with small grains and large electron mean free path ( $L_e$ ) [17]. It should be noted that the Hall effect measures electron transport laterally across the film while SE probes the film in the vertical direction. It is possible that electron transport is not isotropic in these films.

## 5. CONCLUSIONS

We have studied effects of the free electrons on electro-optical properties of CdO thin films doped with different dopants (In, Ga, V, Ti). Samples with carrier concentration ranging from  $2 \times 10^{20} \text{ cm}^{-3}$  to  $12 \times 10^{20} \text{ cm}^{-3}$  were measured using spectroscopic ellipsometry. It was found that free carriers significantly affect the complex dielectric function of doped CdO thin films. Analysis of SE data using a combined Drude and Tauc-Lorentz model provided various material parameters, including refractive index  $n(\lambda)$ , high frequency dielectric constant  $\epsilon_\infty$ , electron mass  $m^*$ , plasma wavelength  $\lambda_p$ , free carrier absorption, optical band gap  $E_G^{\text{opt}}$  and optical mobility  $\mu_{\text{opt}}$ . We observed that with increasing carrier concentration, (i)  $\epsilon_\infty$  decreases roughly linearly from  $\sim 5.6$  to 4.8, (ii)  $\alpha$  in the NIR region increases significantly due to free carrier absorption, (iii) the  $E_G^{\text{opt}}$  increases due to Burstein-Moss and band gap renormalization effects from 2.3 to 3.2 eV, (iv)  $\lambda_p$  decreases, and (v) the  $m^*$  for In and Ga doped CdO increases from  $0.13 m_o$  for electrons at the bottom of the conduction band to  $0.33 m_o$ . The dependence of  $m^*$  on the carrier concentration is consistent with prediction from the nonparabolic conduction band model. For transition metal doped CdO, at high doping ( $N > 8 \times 10^{20} / \text{cm}^3$ ) the  $m^*$  deviates significantly from the nonparabolic model and is  $\sim 20$ -30% higher than that for Ga and In doped materials. This is attributed to the modification of the CdO CB by the interaction of localized d states of the TM dopants with the extended CdO CB state. Our measured results of doped CdO thin films with high mobility, low resistivity, long plasma reflection wavelength, low free electron absorption, large high-frequency dielectric constant and high refractive index make it an ideal transparent conductor

especially when transmission of IR photons ( $\lambda > 1000$  nm) is required.

## ACKNOWLEDGEMENTS

This work was supported by the City University of Hong Kong (project #9380076). Material synthesis and RBS analysis performed at LBNL were supported by the Electronic Materials Program at the Lawrence Berkeley National Laboratory. JAZ acknowledges support by the Research Grants Council, University Grants Committee, Hong Kong (Project No. CityU 122812). Yishu Foo was supported by the Hong Kong PhD Fellowship PF-15139, Research Grants Council, University Grants Committee, Hong Kong.

## FIGURE CAPTIONS

Fig. 1 Electron concentration (a) and mobility (b) for CdO films doped with group III (Ga and In) and transition metal (V and Ti) dopants with increasing dopant concentration. The dash lines are guides to the eyes using simple polynomial fitting of data points.

Fig. 2 The measured (black square) and the fitted (red solid line) SE spectra of CdO:In thin film, with  $N_{Hall} = 6.6 \times 10^{20} \text{ cm}^{-3}$  and angle of incidence of  $70^\circ$ .

Fig. 3 (Color online) the complex dielectric function (a) and the complex refractive index (b) extracted from the optical model for CdO:In thin films with variable  $N_{Hall}$ .

Fig. 4 (Color online) the complex dielectric function of doped (In, Ga, V, Ti) CdO thin film with similar  $N_{Hall}$  (a), and the absorption coefficient of the doped CdO thin films (b). The inset in (b) is the corresponding  $\alpha$  in a smaller energy range (0.74~2.3 eV) in the log scale, with the dotted lines representing the calculated  $\alpha_{FCA}$ . The undoped CdO thin film with  $N_{Hall} \approx 1.29 \times 10^{20} \text{ cm}^{-3}$  is also shown for comparison.

Fig. 5 (Color online) absorption coefficient (a) at wavelength of 1200 nm and the refractive index (b) at wavelength of 600 nm of CdO thin films doped with various dopants (In, Ga, V, Ti) obtained from SE analysis. The refractive index of undoped CdO thin film is also given for reference.

Fig. 6: (Color online) The real part of dielectric function  $\epsilon_1$  (a) plotted as function of  $1/(E^2 + \Gamma_D^2)$ , and the high frequency dielectric constant (b) of CdO thin films with dependence on Hall carrier concentration.

Fig. 7 The plasma wavelength obtained from SE analysis for doped CdO thin films as a function of  $N_{Hall}$ . The previously reported results for other TCOs by Kostlin *et al.* (Ref.40), Jin *et al.* (Ref.41), and Fujiwara *et al.* (Ref. 16) are also shown for comparison.

Fig. 8 Electron effective mass  $m^*$  for CdO thin films with different dopants as a function of  $N_{Hall}$ , where  $m_0$  is the free electron mass. The black line is the best fit

for data from the In and Ga doped samples by using Eq. (11), the dashed lines are fits with fixed  $m_0^*$  with values of 0.1 and  $0.2m_0$ .

Fig. 9 Plotting of  $\alpha^2$  as a function of photon energy for CdO:In films with different  $N_{Hall}$  (a), and optical band gap of doped CdO thin films as a function of  $N_{Hall}$  (b).

Fig. 10: (Color online) Band gap shift of doped CdO thin films as a function of  $N_{Hall}$ , assuming an intrinsic band gap of 2.3 eV. The calculated Burstein-Moss shift  $\Delta E_G^{BM}$ , the band gap renormalization  $\Delta E^{BGN}$ , as well as  $\Delta E_G^{BM} - \Delta E^{BGN}$  are also illustrated.

Fig. 11 (a) Optical mobility ( $\mu_{opt}$ ) obtained from SE analysis using the effective mass presented in Fig. 8, and (b) mean free path of CdO thin films as a function of  $\mu_{Hall}$ .

## REFERENCES

- [1] D. S. Ginley, H. Hosono, and D. C. Paine, *Handbook of Transparent Conductor* (Springer, New York, 2010).
- [2] K. Ellmer, *Past achievements and future challenges in the development of optically transparent electrodes*, Nature Photonics, **6**, 809 (2012).
- [3] C. I. Bright, *50 Years of Vacuum Coating Technology and the Growth of the Society of Vacuum Coaters* (Society of Vacuum Coaters, 2007), Chap. VII.
- [4] T. Minami, *Present status of transparent conducting oxide thin-film development for indium-tin-oxide (ITO) substitutes*, Thin Solid Films **516**, 5822 (2008).
- [5] K. Ellmer, A. Klein, B. Rech (Eds.), *Transparent Conductive Zinc Oxide: Basics and Applications in Thin Film Solar Cells*, Springer, New York, 2008.
- [6] M. Yan, M. Lane, C. R. Kannewurf, and R. P. H. Chang, *Highly conductive epitaxial CdO thin films prepared by pulsed laser deposition*, Appl. Phys. Lett. **78**, 2342 (2001).
- [7] K. M. Yu, M. A. Mayer, D. T. Speaks, H. He, R. Zhao, L. Hsu, S. S. Mao, E. E. Haller, and W. Walukiewicz, *Ideal transparent conductors for full spectrum photovoltaics*, J. Appl. Phys. **111**, 123505 (2012).
- [8] S. G. Choi, J. Z. Perez, V. M. Sanjose, A. G. Norman, C. L. Perkins, and D. H. Levi, *Complex dielectric function and refractive index spectra of epitaxial CdO thin film grown on r-plane sapphire from 0.74 to 6.45 eV*, J. Vac. Sci. Technol. B **28**, 1120 (2010).
- [9] C. E. Ekuma, J. Moreno, and M. Jarell, *Electronic, transport, optical and structural properties of rocksalt CdO*, J. Appl. Phys. **114**, 153705 (2013).
- [10] S. K. V. Farahani, T. D. Veal, P. D. C. King, J. Z. Perez, V. M. Sanjose, and C. F. McConville, *Electron mobility in CdO films*, J. Appl. Phys. **109**, 073712 (2011).
- [11] S. Jin, Y. Yang, J. E. Medvedeva, L. Wang, S. Li, N. Cortes, J. R. Ireland, A. W. Metz, J. Ni, M. C. Hersam, A. J. Freeman, and T. J. Marks, *Tuning the properties of transparent oxide conductors dopant ion size and electronic structure effects on CdO-based transparent conducting oxide Ga-and In-doped CdO thin film grown by MOCVD*, Chem. Mater. **20**, 220 (2008).
- [12] J. J. Mudd, T. L. Lee, V. M. Sanjose, J. Zuniga Perez, D. Hesp, J. M. Kahk, D. J. Payne, R. G. Egdell, and C. F. McConville, *Hard x-ray photoelectron spectroscopy as a probe of the intrinsic electronic properties of CdO*, Phys. Rev. B **89**, 035203 (2014).
- [13] I. N. Demchenko, M. Chernyshova, T. Tyliczszak, J.D. Denlinger, K. M. Yu, D. T.

- Speaks, O. Hemmers, W. Walukiewicz, G. Derkachov, K. L. Jablonska, *Electronic structure of CdO studied by soft x-ray spectroscopy*, Journal of Electron Spectroscopy and Related Phenomena **184**, 249 (2011).
- [14] M. Burbano, D. O. Scanlon, and G. W. Watson, *Source of conductivity and doping limits in CdO from hybrid density functional theory*, J. Am. Chem. Soc. **133**, 15065 (2011).
- [15] Kin Man Yu, D. M. Detert, Guibin Chen, Wei Zhu, Chaoping Liu, S. Grankowska, O. D. Dubon, Leon Hsu, and Wladek Walukiewicz, *Defects and Properties of Cadmium Oxide Based Transparent Conductors*, J. Appl. Phys. **119**, 181501 (2016).
- [16] H. Finkenrath and N. Uhie, *Der Einfluss Der Gitterschwingungen Auf Die Ultrarot-Reflexion Von CdO*, Solid State Communications, **5**, 875 (1967).
- [17] R. J. Mendelsberg, Y. Zhu and A. Anders, *Determining the nonparabolicity factor of the CdO conduction band using indium doping and the Drude theory*, J. Phys. D: Appl. Phys. **45**, 425302 (2012).
- [18] M. Fox, *Optical Properties of Solids* (Oxford University Press, New York, 2010).
- [19] H. Fujiwara, and M. Kondo, *Effects of carrier concentration on the dielectric function of ZnO:Ga and In<sub>2</sub>O<sub>3</sub>:Sn studied by spectroscopy ellipsometry: Analysis of free-carrier and band-edge absorption*, Phys. Rev. B **71**, 075109 (2005).
- [20] J. A. Stoke, J. D. Beach, W. C. Bradford, T. R. Ohno, *Electrical and optical properties of magnetron sputtered Cd<sub>2</sub>SnO<sub>4</sub> transparent conducting oxide thin films for use in CdTe solar devices*, Thin Solid Films **562**, 254 (2014).
- [21] P. P. Edwards, A. Porch, M. O. Jones, D. V. Morgan and R. M. Perks, *Basic materials physics of transparent conducting oxides*, Dalton Trans. 2995 (2004).
- [22] T. Yamada, H. Makino, N. Yamamoto, and T. Yamamoto, *Ingrain and grain boundary scattering effects on electron mobility of transparent conducting polycrystalline Ga-doped ZnO films*, J. Appl. Phys. **107**, 123534 (2010).
- [23] I. Hamberg and C. G. Granqvist, *Evaporated Sn-doped In<sub>2</sub>O<sub>3</sub> films: basic optical properties and applications to energy efficient windows*, J. Appl. Phys. **60**, R123 (1986).
- [24] Z. C. Jin, I. Hamberg, and C. G. Granqvist, *Optical properties of sputter-deposited ZnO:Al thin films*, J. Appl. Phys. **64**, 5117 (1988).
- [25] Y. Qu, T. A. Gessert, K. Ramanathan, R. G. Dhere, R. Noufi, and T. J. Coutts, *Electrical and optical properties of ion beam sputtered ZnO:Al as a function of film thickness*, J. Vac. Sci. Technol. A **11**, 996 (1993).
- [26] D. E. Aspnes, *Spectroscopic ellipsometry-Past, present, and future*, Thin Solid Films **571**, 334 (2014).
- [27] H. G. Tompkins and E. A. Irene (Eds), *Handbook of Ellipsometry* (Springer-Verlag, Berlin, 2005).
- [28] M. Feneberg, J. Nixdorf, C. Lidig, R. Goldhahn, Z. Galazka, O. Bierwagen, J. S. Speck, *Many-electron effects on the dielectric function of cubic In<sub>2</sub>O<sub>3</sub>: Effective electron mass, band nonparabolicity, band gap renormalization, and Burstein-Moss shift*, Phys. Rev. B **93**, 045203 (2016).
- [29] R. A. Synowicki, *Suppression of backside reflections from transparent substrates*, Phys. Stat. Sol. C **5**, 1085 (2008).
- [30] J. Lee, P. I. Rovira, I. An, and R. W. Collins, *Rotating-compensator multichannel ellipsometry: Applications for real time Stokes vector spectroscopy of thin film*

- growth, Rev. Sci. Instrum. **69**, 1800 (1998).
- [31] J. A. Woollam Co., Inc., *Guide to Using WVASE32<sup>®</sup>* (2008).
  - [32] D. E. Aspnes, Optical properties of thin films, Thin Solid Films **89**, 249 (1982).
  - [33] P. I. Rovira and R. W. Collins, Analysis of specular and textured SnO<sub>2</sub>:F by high speed four-parameter Stokes vectors spectroscopy, J. Appl. Phys. **85**, 2015 (1999).
  - [34] T. Yamada, H. Makino, N. Yamamoto, and T. Yamamoto, *Ingrain and grain boundary scattering effects on electron mobility of transparent conducting polycrystalline Ga-doped ZnO films*, J. Appl. Phys. **107**, 123534 (2010).
  - [35] E. Shanthi, V. Dutta, A. Banerjee, and K. L. Chopra, J. Appl. Phys. **51**, 6243 (1980).
  - [36] E. Shanthi, A. Banerjee, V. Dutta, and K. L. Chopra, J. Appl. Phys. **53**, 1615 (1982).
  - [37] G. E. Jellison Jr, and F. A. Modine, *Parameterization of the optical functions of amorphous materials in the interband region*, Appl. Phys. Lett. **69**, 371 (1996), Erratum, Appl. Phys. Lett. **69**, 2137 (1996).
  - [38] J. M. Langer, C. Delerue, M. Lannoo, and H. Heinrich, *Phys. Rev. B* **38**, 7723 (1988).
  - [39] F. Ruske, Deposition and Properties of TCOs, in W. G. J. H. M. van Sark, L. Korte, F. Roca (Ed.), *Physics and Technology of Amorphous-Crystalline Heterostructure Silicon Solar Cells* (Springer Berlin Heidelberg, 2012).
  - [40] B. R. Bennett, R. A. Soref, and J. A. Del Alamo, Carrier-induced change in refractive index of InP, GaAs and InGaAsP, IEEE J. Quant. Elect. **26**, 113 (1990).
  - [41] J. Poortmans and V. Arkhipov (Ed.), *Thin Film Solar Cells: Fabrication, Characterization and Applications* (John Wiley & Sons, Ltd, Chichester, 2006).
  - [42] H. Finkenrath, H. Kohler, M. Lochmann, *Z. Angew. Phys.* **21**, 512 (1966).
  - [43] H. Kostlin, R. Jost, and W. Lems, *Phys. Status Solidi A* **29**, 87 (1975).
  - [44] Z. C. Jin, I. Hamberg, and C. G. Granqvist, J. Appl. Phys. **64**, 5117 (1988).
  - [45] T. Pisarkiewicz, K. Zakrzewska, and E. Leja, Thin Solid Films **174**, 217 (1989).
  - [46] T. Pisarkiewicz and A. Kolodziej, *Nonparabolicity of the conduction band structure in degenerate tin dioxide*, *Phys. Status Solidi B* **158**, K5 (1990).
  - [47] Y. Dou, T. Fishlock, R. G. Egdell, D. S. L. Law, and G. Beamson, *Phys. Rev. B* **55**, R13381 (1997).
  - [48] T. J. Coutts, D. L. Young, X. Li, W. P. Mulligan and X. Wu, *J. Vac. Sci. Technol. A* **18**, 2646 (2000).
  - [49] P. H. Jefferson, S. A. Hatfield, T. D. Veal, P. D. C. King, C. F. McConville, J. Z. Perez and V. M. Sanjose, *Appl. Phys. Lett.* **92**, 022101 (2008).
  - [50] J. A. Woollam, W. A. McGahan and B. Johs, *Spectroscopic ellipsometry studies of indium tin oxide and other flat panel display multilayer materials*, Thin Solid films, **241**, 44 (1994).
  - [51] N. Preissler, O. Bierwagen, A. T. Ramu, J. S. Speck, *Electrical transport, electrothermal transport, and effective electron mass in single-crystalline In<sub>2</sub>O<sub>3</sub> films*, *Phys. Rev. B* **88**, 085305 (2013).
  - [52] A. V. Singh, R. M. Mehra, A. Yoshida, and A. Wakahara, *Doping mechanism in aluminum doped zinc oxide films*, J. Appl. Phys. **95**, 3640 (2004).

- [53] T. Nagatomo, Y. Maruta, and O. Omoto, *Electrical and optical properties of vacuum evaporated indium-tin oxide films with high electron mobility*, Thin Solid Films, 192, 17 (1990).
- [54] E. García-Hemme, K. M. Yu, P. Wahnón, G. González-Díaz, W. Walukiewicz, Effects of d-donor level of vanadium on the properties of  $\text{Zn}_{1-x}\text{V}_x\text{O}$  films, Appl. Phys. Lett., **106**, 182101 (2015).
- [55] Y. Ohhata, F. Shinoki, and S. Yoshida, Optical properties of R.F. reactive sputtered tin-doped  $\text{In}_2\text{O}_3$  films, Thin Solid Films 59, 255 (1979).
- [56] I. Hamberg, C. G. Granqvist, K. F. Berggren, B. E. Sernelius, L. Engstrom, Phys. Rev. B **30**, 3240 (1984)
- [57] B. E. Sernelius, K. F. Berggren, Z. C. Jin, I. Hamberg, C. G. Granqvist, Phys. Rev. B **37**, 10244 (1988).
- [58] Y. Zhu, R. J. Mendelsberg, J. Zhu, J. Han, A. Anders, Structural, optical and electrical properties of indium-doped cadmium oxide films prepared by pulsed filtered cathodic arc deposition, J. Mater. Sci. 48, 3789 (2013).
- [59] S. C. Jain, J. M. McGregor, D. J. Roulston, J. Appl. Phys. 68, 3747 (1990)
- [60] S. C. Jain, D. J. Roulston, Solid-State Electron 34, 453 (1991).
- [61] C. Kittel, *Introduction to Solid State Physics* (Seventh Edition, Wiley, New York, 1996).
- [62] T. Yamanoto, T. Sakemi, K. Awai, S. Shirakata, *Dependence of carrier concentrations on oxygen pressure for Ga-doped ZnO prepared by ion plating method*, Thin Solid Films **451-452**, 439 (2004).
- [63] M. Akagawa, and H. Fujiwara, *Optical characterization of textured  $\text{SnO}_2\text{:F}$  layers using spectroscopic ellipsometry*, J. Appl. Phys. **112**, 083507 (2012).